UC Berkeley
UC Berkeley Previously Published Works

Title

Telomere length set point regulation in human pluripotent stem cells critically depends on the shelterin protein TPP1

Permalink

https://escholarship.org/uc/item/08b0690x

Journal

Molecular Biology of the Cell, 31(23)

ISSN

1059-1524

Authors

Boyle, John M
Hennick, Kelsey M
Regalado, Samuel G
et al.

Publication Date

2020-11-01

DOI

10.1091/mbc.e19-08-0447

Copyright Information

Peer reviewed

Telomere length set point regulation in human pluripotent stem cells critically depends on the shelterin protein TPP1

John M. Boyle[a], Kelsey M. Hennick[a], Samuel G. Regalado[a], Jacob M. Vogan[a], Xiaozhu Zhang[a], Kathleen Collins[a], and Dirk Hockemeyer[a,b,c,*]

[a]Department of Molecular and Cell Biology and [c]Innovative Genomics Institute, University of California, Berkeley, Berkeley, CA 94720; [b]Chan Zuckerberg Biohub, San Francisco, CA 94158

ABSTRACT Telomere maintenance is essential for the long-term proliferation of human pluripotent stem cells, while their telomere length set point determines the proliferative capacity of their differentiated progeny. The shelterin protein TPP1 is required for telomere stability and elongation, but its role in establishing a telomere length set point remains elusive. Here, we characterize the contribution of the shorter isoform of TPP1 (TPP1S) and the amino acid L104 outside the TEL patch, TPP1's telomerase interaction domain, to telomere length control. We demonstrate that cells deficient for TPP1S (TPP1S knockout [KO]), as well as the complete TPP1 KO cell lines, undergo telomere shortening. However, TPP1S KO cells are able to stabilize short telomeres, while TPP1 KO cells die. We compare these phenotypes with those of TPP1$^{L104A/L104A}$ mutant cells, which have short and stable telomeres similar to the TPP1S KO. In contrast to TPP1S KO cells, TPP1$^{L104A/L104A}$ cells respond to increased telomerase levels and maintain protected telomeres. However, TPP1$^{L104A/L104A}$ shows altered sensitivity to expression changes of shelterin proteins suggesting the mutation causes a defect in telomere length feedback regulation. Together this highlights TPP1$^{L104A/L104A}$ as the first shelterin mutant engineered at the endogenous locus of human stem cells with an altered telomere length set point.

Abbreviations used: acd, adrenocortical dysplasia; BSA, bovine serum albumin; DDR, DNA damage response; hESC, human embryonic stem cell; hPSC, human pluripotent stem cell; iPSC, induced pluripotent stem cell; KO, knockout; M, methionine; OD, optical density; PBS, phosphate-buffered saline; TBS, Tris-buffered saline; TIF, Telomere Dysfunction-Induced Foci; TRAP, telomeric repeat amplification protocol; TRF, telomere restriction fragment.

INTRODUCTION

Telomere length maintenance is essential in human stem cells for long-term proliferation and thus is linked to the renewal capacity of human cells and tissues (Aubert and Lansdorp, 2008). The enzyme telomerase catalyzes the addition of telomeric repeats to the chromosome end (Greider and Blackburn, 1985, 1989; Hemann *et al.*, 2000), thereby counteracting the terminal sequence loss due to the end replication problem and nucleolytic degradation. Most somatic cells down-regulate telomerase and thus lose the ability to prevent progressive telomere shortening. Shortened telomeres eventually lead to the induction of a DNA damage signal and cellular arrest or cell death (Hayflick, 1965; Harley *et al.*, 1990; d'Adda di Fagagna *et al.*, 2003). This proliferation barrier functions as a robust tumor suppression mechanism (Shay, 2016).

Human embryonic stem cells (hESCs) and induced pluripotent stem cells (iPSCs), collectively referred to as human pluripotent stem cells (hPSCs), resemble cells of the early human embryo that are telomerase positive and immortal (Thomson *et al.*, 1998; Takahashi *et al.*, 2007). In contrast to differentiated somatic cells, hESCs maintain telomeres within a defined range, referred to as the "telomere

length set point" (Greider, 1996) of approximately 9–12 kb (Thomson *et al.*, 1998; Rivera *et al.*, 2016). Analogously, iPSCs reset their telomeres to a similar length during the reprogramming process (Marion *et al.*, 2009; Batista *et al.*, 2011; Batista and Artandi, 2013). Telomere length also resets to wild-type levels after TERT expression is restored in hESCs harboring TERT deletions (Chiba *et al.*, 2015, 2017). This restoration to a stem cell-specific telomere length set point provides evidence that the telomere length maintenance in stem cells is distinct from merely counteracting telomere shortening and maintaining telomeres at homeostasis. To maintain homeostasis, a balance must exist between telomere sequence loss during DNA replication and de novo repeat addition. To establish homeostasis at a specific telomere length set point, stem cells must sense the total telomeric sequence present at a chromosome end, integrate this information with telomerase levels, and mediate its access to the chromosome end. It is important to note that such a defined telomere length set point is a specific feature of stem but not cancer cells. In cells of the same tumor type (Ceccarelli *et al.*, 2016; Hayward *et al.*, 2017) and subclones as well as second-round subclones of cancer cell lines, telomere length can differ substantially (Bryan *et al.*, 1998). Based on experiments in model organisms and cancer cells, it has been postulated that homeostasis is maintained by balancing telomeres between a telomerase extendable state and a nonextendable state (Teixeira *et al.*, 2004), which can be modulated depending on the presence of the shelterin complex at the telomere (van Steensel and de Lange, 1997; Cristofari and Lingner, 2006; Hug and Lingner, 2006; Hockemeyer and Collins, 2015).

Overexpression and knockdown studies have been used to elucidate the mechanism by which the shelterin complex regulates the telomere length. The shelterin complex is comprised of six protein subunits (TRF1, TRF2, Rap1, TIN2, TPP1, and POT1) that are specifically recruited to the telomeric repeat array (de Lange, 2005; Schmutz and de Lange, 2016). This complex is required to protect the chromosome ends from an aberrant DNA damage response (DDR; de Lange, 2010) and is required for telomere maintenance by telomerase. TRF1 and TRF2 bind to the double-stranded telomeric repeats and have been shown to act as negative regulators of telomere length (van Steensel and de Lange, 1997; Smogorzewska *et al.*, 2000). TRF1 and TRF2 are bridged by TIN2. TIN2 acts to recruit TPP1 (Houghtaling *et al.*, 2004; Liu *et al.*, 2004; Ye *et al.*, 2004b) and its binding partner, POT1. POT1 can bind single-stranded telomeric DNA through its N-terminal OB-fold domains and controls telomerase access to the 3′-OH (reviewed in Hockemeyer and Collins, 2015).

In its position between TIN2 and POT1, TPP1 can act to mediate telomere length signals coming from TRF1 and TRF2 and pass them to POT1 and telomerase. TPP1 is the only shelterin component shown to directly interact with telomerase through a motif referred to as the TEL patch. This interaction is essential for the recruitment of telomerase to telomeres (Wang *et al.*, 2007; Xin *et al.*, 2007; Nandakumar *et al.*, 2012; Zhong *et al.*, 2012; Schmidt *et al.*, 2014; Sexton *et al.*, 2014; Hockemeyer and Collins, 2015).

hESCs harboring endogenous deletions of the acidic loop of TPP1's TEL patch (TPP1$^{\Delta L/\Delta L}$) show telomere shortening at rates that phenocopy those of telomerase knockout (KO) hESCs (Sexton *et al.*, 2014). Complementation of TPP1$^{\Delta L/\Delta L}$ hESCs with wild-type TPP1 restored telomere length to the length of wild-type hESCs. However, expression of a TPP1 variant containing a single amino acid substitution at position 104 (TPP1^{L104A}) outside of the TEL patch (Nandakumar *et al.*, 2012; Grill *et al.*, 2018) can rescue the long-term viability of TEL patch-deficient cells but it fails to reset telomere length to wild-type hESC levels (Sexton *et al.*, 2014). The TPP1

mutant was initially described in an in vitro assay using purified TPP1 fragments missing the TIN2 binding domain (Nandakumar *et al.*, 2012). This fragment was shown to have a defect in stimulating telomerase processivity in vitro. However, when tested in the context of full-length TPP1 in vivo, TPP1^{L104A} was capable of recruiting telomerase (Sexton *et al.*, 2014). Subsequent in vitro experiments showed only an insignificant decrease in the ability of TPP1^{L104A} to stimulate telomerase processivity when compared with wild-type TPP1 (Grill *et al.*, 2018). Collectively these findings leave open the question of whether the TPP1^{L104A} mutation changes telomere length by affecting the amount of repeat synthesis by each telomere-bound telomerase enzyme or instead by altering the balance of telomere states that determines telomere length set point.

Previous telomere set point control experiments, including our own, were limited by using overexpression of TPP1 alleles. Here, we dissect the role of TPP1 in telomere length set point control by comparing TPP1 alleles genetically engineered at the endogenous TPP1 locus. Specifically, we contrasted the loss of function phenotypes of TPP1 with the phenotypes of cell lines containing endogenous homozygous TPP1^{L104A} mutations (TPP1$^{L104A/L104A}$). This approach allowed us to demonstrate that TPP1^{L104A} is not a hypomorphic allele. The full TPP1 KO and KO of the short isoform of TPP1 were compromised in telomere protection. In contrast, TPP1$^{L104A/L104A}$ hESCs are capable of telomere end protection and telomere length homeostasis, despite having very short telomeres. This indicates that TPP1^{L104A} is competent to recruit and activate telomerase as well as to tether POT1 to telomeres. However, TPP1$^{L104A/L104A}$ hESCs show a pronounced defect in the stem cell-specific telomere length set point and only maintain very short telomeres. Moreover, overexpressing of well-characterized alleles of sheltering proteins in TPP1$^{L104A/L104A}$ hESCs revealed that the TPP1^{L104A} mutation causes a blunted response to telomere length cues necessary to establish the hESC-specific telomere length set point.

RESULTS

The human ACD (TPP1) locus expresses two isoforms in hESCs

TPP1 has several annotated splice variants. Recent polysome profiling and Transcript Isoforms in Polysomes sequencing (TrIP-seq; Floor and Doudna, 2016; Blair *et al.*, 2017) experiments suggest that hESCs translate at least two isoforms of TPP1, a long isoform TPP1L (ENST00000393919), which starts translation at base pair 338 of the longest NCBI annotated transcript, and a second more abundant short isoform TPP1S (ENST00000620761), which is generated from a different transcript with a translational start site 258 base pairs downstream of TPP1L's ATG (Figure 1A and Supplemental Figure S1A). This downstream ATG encodes methionine 87 in the long transcript; hence, we refer to it as M87, where the first ATG in this transcript is referred to as M1 (Figure 1, A and B). To address how TPP1S contributes to telomere protection and length control, we mutated its ATG start codons using CAS9-mediated genome editing (Jinek *et al.*, 2012). We engineered two heterozygous cell lines with a monoallelic knock-in of the repair template, changing the short ATG to ATT (TPP1$^{M87I/+}$) and one compound heterozygous cell line with a monoallelic knock-in and disruption of the other allele (TPP1$^{M87I/-}$, referred to as TPP1S KO). We also generated cell lines harboring either monoallelic or biallelic mutation at the first ATG (TPP1$^{\Delta M1/+}$ and TPP1$^{\Delta M1/\Delta M1}$) (Supplemental Figure S1B). TPP1S KO cells remained pluripotent based on the expression of the pluripotency marker OCT4 (Figure 1C) and initially proliferated indistinguishably from unedited control clones and untargeted wild-type cells (Figure 1D). Western blot analysis of the TPP1S KO cells

confirmed the absence of the TPP1S protein. In contrast, mutation of the TPP1L ATG did not result in the depletion of a specific protein species. This could be due to translational initiation on a downstream ATG coding for a methionine at amino acid 11. Consistent with this, computational analysis using the *ATG*pr (http://atgpr .dbcls.jp/) software shows an increased probability that M11 is used as a translational start site of a TPP1L transcript carrying the M1 mutation. We did not detect any phenotype associated with the homozygous mutation of M1 and therefore focused on the analysis of the TPP1S KO (Supplemental Figure S1B).

Loss of TPP1S leads to telomere shortening and deprotection

To assess the proliferative capacity of the TPP1S KO, we monitored cellular proliferation and telomere length (Figure 1, E–G) over time. Initially, TPP1S KO cells grew at a rate indistinguishable from wild-type cells. However, at ~165 d posttargeting, TPP1S KO hESC cultures started to proliferate slower (Figure 1G), resulting in smaller stem cell colonies, significantly lower cell numbers, and increased numbers of dead cells. This phenotype was highly reminiscent of late passage TERT$^{-/-}$ cells and the telomerase recruitment mutant, TPP1$^{\Delta L/\Delta L}$, cells (Sexton *et al.*, 2014). In contrast to TERT$^{-/-}$ and TPP1$^{\Delta L/\Delta L}$, TPP1S KO cultures continued to proliferate, but slower than wild-type control cells. Following 9 wk of reduced proliferation, TPP1S KO cultures returned to a rate similar to wild-type cells. To rule out cross-contamination, TPP1S KO was reconfirmed by genotyping PCR and Western blot analysis of long-term cultures after wild-type proliferation rates had recovered (Figure 1D). The parallel culture of TPP1$^{\Delta M1/\Delta M1}$ hESCs proliferated continuously at the same rate as wild-type cells.

Next, we analyzed the telomere length changes in TPP1S KO cells over time. This analysis revealed pronounced telomere shortening in TPP1S KO cells over the first 184 d. However, telomere shortening eventually slowed, and mean telomere length stabilized at approximately 3.5 kb, and from there on telomere length remained stable. Next, we investigated the role of TPP1S KO in suppressing telomere DDR by quantifying the frequency of Telomere Dysfunction-Induced Foci (TIFs). TIFs were very infrequent in wild-type control but readily detectable in TPP1S KO cells (Figure 1, H and I).

Targeted disruption of all predicted TPP1 isoforms leads to phenotypes different from the TPP1S KO

Our observation that TPP1S KO cells are viable suggests that another protein product present in TPP1S KO cells is sufficient to execute the essential functions of TPP1. To test this, we attempted to completely KO TPP1. Out of four rounds of gene targeting resulting in 245 clones with three different strategies to KO TPP1 in wild-type cells, we were unable to isolate a single TPP1 KO clone. We hypothesized that the failure to KO TPP1 was the result of DNA damage checkpoint activation and p53-response (Kibe *et al.*, 2010; Tejera *et al.*, 2010). Therefore, we repeated the KO in an hESC line with impaired cell cycle and DNA damage checkpoints. We used a genetically engineered hESC line with a biallelic deletion of exon two of CDKN2A, which inactivates both p14 and p16 (Chiba *et al.*, 2017). In this cell line, we also disrupted the *TERT* locus and complemented this loss by introducing a loxP-flanked hTERT expression cassette into the *AAVS1* locus. Using this cell line, we were able to derive one single TPP1 KO hESC clone that carried a homozygous integration of a PGK-PURO cassette (TPP1 $^{E2–Puro/E2–Puro}$), which is predicted to result in the complete loss of TPP1 expression (Figure 2, A and B; Supplemental Figure S2). Telomeres in this clone rapidly

shortened, resulting in cell death after approximately 87–120 d (Figure 2C).

In comparison, loop out of the TERT transgene resulted in cell death after 118, 131, and 145 d in three independent clones, respectively (Figure 2D). These data suggest that the telomere shortening observed in TPP1-deficient cells could be the result of not only a lack of telomerase recruitment but also exacerbated by the loss of telomere protection. As expected, staining for γ-H2AX and TRF1 confirmed the presence of TIFs in the TPP1$^{E2–Puro/E2–Puro}$ cells (Figure 2, E and F). TPP1 is essential for long-term stem cell viability; this is consistent with previous studies (Sexton *et al.*, 2014; Kim *et al.*, 2017).

TPP1^{L104A} is a novel telomere length set point mutant

In contrast to the cell death seen in the full TPP1 KO, the TPP1S KO cells were able to maintain short telomeres. The telomere length set point of the TPP1S KO after the long-term culture is reminiscent of the telomere length phenotype we previously identified when the TPP1^{L104A} allele was overexpressed in TPP1$^{\Delta L/\Delta L}$ cells. TPP1^{L104A} was able to restore long-term viability in TPP1$^{\Delta L/\Delta L}$ but resulted in uncharacteristically short telomeres for stem cells (Sexton *et al.*, 2014). These complementation assays by overexpression did not completely resolve the question of whether TPP1^{L104A} is a hypomorphic loss of function allele or acts as a neomorphic allele when expressed endogenously. To fully characterize this mutant and to determine whether TPP1$^{L104A/L104A}$ will act similarly as TPP1S KO, we edited the endogenous TPP1 locus changing leucine 104 to alanine (Supplemental Figure S3, A and B). Telomere length showed that the homozygous TPP1$^{L104A/L104A}$ substitution at the endogenous TPP1 locus results in the gradual loss of telomeric signal (Figure 3, A and B; Supplemental Figure S3C). Telomeric repeats were lost over 130 d following editing and finally stabilized at a mean telomere length of approximately 3.5 kb. This telomere shortening phenotype was confirmed by a second compound heterozygous clone, TPP1$^{L104A/–}$ (Supplemental Figure S3C). Notably, the final telomere length and size distribution of TPP1$^{L104A/L104A}$ was comparable to those ultimately seen in TPP1S KO cells. Importantly, we confirmed the specificity of the TPP1$^{L104A/L104A}$ telomere length phenotype by genetically reverting the defect and repairing TPP1$^{L104A/L104A}$ to TPP1$^{A104L/A104L}$. This restoration of endogenous wild-type TPP1 expression did not impact protein abundance but resulted in the rapid reestablishment of the telomere length to the hESC specific set point, confirming the specificity of the TPP1$^{L104A/L104A}$ phenotype (Figure 3, C and D, lanes 6 and 7).

To confirm the L104A allele is not a hypomorphic loss of function allele that can be overcome by merely increasing TPP1^{L104A} abundancy, we overexpressed TPP1 alleles from the *AAVS1* locus in wild-type and TPP1$^{L104A/L104A}$ hESCs. Overexpression of TPP1S^{L104A} or TPP1S$^{\Delta L}$, a TEL-patch loop deletion mutant, failed to rescue the short telomere phenotype seen in TPP1$^{L104A/L104A}$ mutant cells (Supplemental Figure S3D), whereas overexpression of wild-type TPP1S restored telomere length to the hESC telomere length set point (Figure 4, A and B). This failure to restore telomere length by TPP1S^{L104A} cannot be explained by the reduced overexpression of this variant, as TPP1S^{L104A} was overexpressed more than sixfold when compared with the endogenous TPP1 levels in this cell line (Figure 4, B and C).

Telomeres are deprotected in TPP1S KO, but not homozygous TPP1^{L104A}, hESCs

Since the new telomere set points and the overall telomere length distribution of both L104A and TPP1S KO cells were approximately
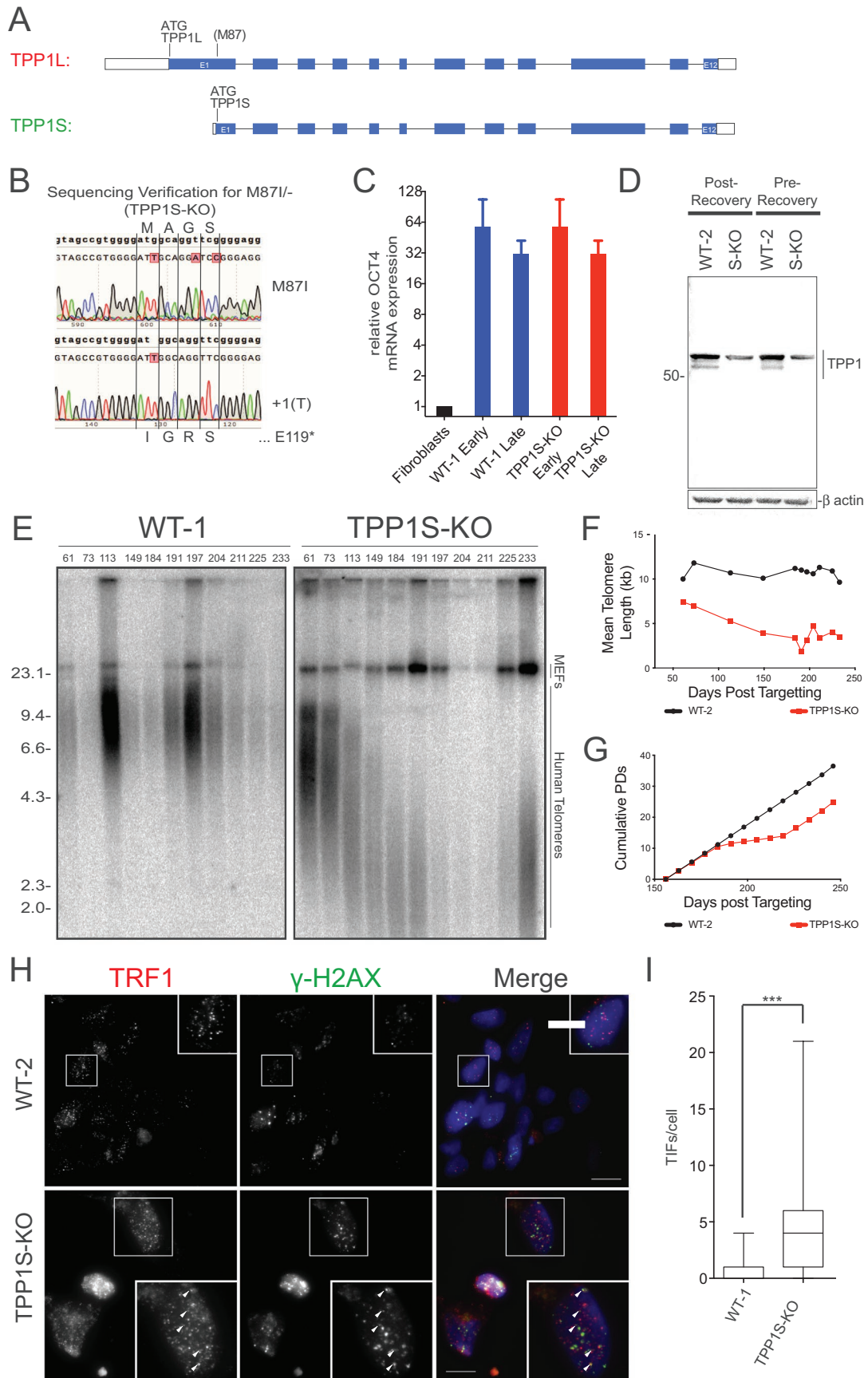
the same, we asked whether TPP1$^{L104A/L104A}$ also has deprotected telomeres. We assessed telomere protection by quantifying TIFs in TPP1$^{L104A/L104A}$ and TPP1S KO cells. TPP1$^{L104A/L104A}$ cells showed wild-type levels of TIF-positive cells (Figure 4, D and E), while TPP1S KO cells had significantly higher levels of TIFs (Figure 2, E and F). We overexpressed a TPP1 variant missing the POT1-binding domain (TPP1^{ΔPBD}) from the AAVS1 locus to act as a positive control for TIF-positive cells (Sexton et al., 2014) (Figure 4, D and E). The expression of this TPP1 variant increased TIF-positive cells in wild-type and TPP1$^{L104A/L104A}$ cells. These results indicate that TPP1$^{L104A/L104A}$ is sufficient to protect short telomeres from a DDR. While telomere length is consistent between TPP1S KO and L104A cells, only the TPP1S KO showed telomere deprotection. These results show that the L104A allele is a novel telomere length set point mutant not a general hypomorphic allele defective in telomere protection as well.

## Telomerase levels increase over time in TPP1S KO cells but not TPP1^{L104A} cells

Both hESC lines, TPP1$^{L104A/L104A}$ and TPP1S KO, have shortening telomeres that eventually reach homeostasis at approximately 3.5 kb. Thus, in the beginning, there is a net loss of telomeric DNA, but over time telomere repeat addition increases to a level that is sufficient to establish homeostasis. Next, we investigated the changes in telomerase activity over time. Telomerase activity can be measured indirectly using telomeric repeat amplification protocol (TRAP). In TRAP, telomeric repeat primers are added to nuclear extracts and subsequently radioactively labeled and amplified by PCR. The detected PCR products correspond to the telomerase activity of each cell line. We performed TRAP assays of early and late TPP1S KO cells. In both TPP1S KO and TPP1$^{L104A/L104A}$, telomerase levels did not decrease, establishing that the telomere shortening is not the consequence of a dramatic reduction in telomerase activity. On the contrary, the telomerase activity of TPP1S KO cells increased over time. The onset of this increase coincided with the observed reduction in proliferation.

Telomerase levels remained elevated at later time points following the restoration of their proliferation rate similar to that observed in wild type. This increase suggests that TPP1S KO cells compensate for the reduced TPP1 function by increased telomerase levels (Figure 5A). In contrast, telomerase activity changes in TPP1$^{L104A/L104A}$ cells were less pronounced and within the range of the activity changes seen in wild-type cells. Therefore, TPP1$^{L104A/L104A}$ cells stabilize telomeres without changing the overall telomerase levels, suggesting a different mechanism by which telomere length stabilizes (Figure 5B).

TPP1 L104 and TPP1S KO show distinct response to telomere elongating cues

So far, our data identified distinct differences between TPP1$^{L104A/L104A}$ mutant and the TPP1S KO cell lines despite their similar telomere length and distribution. Next, we asked if both mutants responded similarly to expression changes in shelterin proteins that are known to perturb telomere length homeostasis. Overexpression of either POT1ΔOB, an allele of POT1 that lacks the first OB-fold required for DNA binding (Loayza and de Lange, 2003), or simultaneous expression of hTERT and hTR from the AAVS1 locus leads to rapid telomere elongation in wild-type cells (Figure 6A and Supplemental Figure S4, A and B) (Hockemeyer et al., 2009, 2011; Chiba et al., 2015). Although TPP1S KO cells showed telomere elongation after either POT1ΔOB or telomerase expression, the response was severely muted. Overexpressing the same alleles in TPP1$^{L104A/L104A}$ cells led to a more complex outcome: overexpression of telomerase leads to fast telomere elongation, driving telomeres beyond the set point of wild-type cells. This was different from the expression of POT1ΔOB, where telomeres slowly elongated but did not fully recover to the wild-type telomere length set point (Figure 6A and Supplemental Figure S4B). This failure of TPP1$^{L104A/L104A}$ cells to appropriately respond to changes in shelterin became also evident when analyzing the telomere elongation following overexpression of a dominant-negative form of TRF1 missing the acidic and

FIGURE 1: Targeted genome editing of the ACD locus. (A) Schematic of the TPP1L, transcript ID ENST00000393919, and TPP1S transcript ID ENST00000620761. TPP1S is in frame with TPP1L and begins at the ATG 258 base pairs downstream from the start codon used by TPP1L. (B) Sanger sequencing verification of mutations at the ATG of TPP1S KO cell lines. The bold lettering above each trace indicated the reference sequence. The capital letter above each trace indicates the sequence of each allele with a vertical line to indicate the reading frame starting at M87. The annotation above and below the traces indicates the amino acid transcribed by each allele where E119* indicated a premature stop on that allele. (C) Relative expression of the pluripotency marker OCT4 determined by qRT-PCR analysis in early- and late-stage wild-type and TPP1S KO cells compared with human fibroblasts (OCT4 negative). Each sample was normalized to GAPDH expression. Early samples were collected before noticeable proliferation defect on days 94, 113, and 120 following targeting. Late samples were collected after proliferation had stabilized on days 225, 240, and 261 following targeting. (D) Western blot analysis of TPP1 gene products shows loss of TPP1S protein bands in TPP1S KO as well as retention of all bands in wild type. Note the disappearance of the shorter product band in lanes two and four have the molecular weight corresponding to TPP1S; the molecular weight of the remaining band corresponds to TPP1L (see Figure 2B; both bands are absent in the complete TPP1 KO). Protein samples were collected from cells 80 and 246 d following targeting. Numbers along the side indicate molecular weight in kilodaltons. (E) Telomere restriction fragment (TRF) analysis monitoring telomere length changes in wild-type and TPP1S KO cell lines over time. The uneven loading of TPP1S KO lanes labeled 197–225 is the result of the limited availability of materials at these time points. Numbers along the top indicate the days postelectroporation with targeting plasmid. Numbers along the side indicate fragment size in kilobases. (F) Quantification of telomere length changes shown in E. (G) Proliferation changes in TPP1S KO cell line compared with wild type. Changes in doubling time were calculated based on the differences in split ratios used during passaging TPP1S KO cells vs. WT-2 cells. Population doubling times were measured by taking the inverse of the fraction of cell passaged taken to the power of two. This number was added to the previous passages to give "cumulative population doublings" (Cumulative PDs). (H) Telomere-dysfunction induced foci (TIF) analysis of wild-type and TPP1S KO cell lines. Arrows indicate the colocalization of TRF1 and γ-H2Ax foci. Scale bars = 10 μm. Samples were collected in parallel after recovery from proliferation defect on day 274 following targeting. (I) Quantification of coincident foci represented in H. Significant determined by Mann–Whitney test, n = 65 WT-1; n = 29 TPP1S KO. Boxes indicate interquartile range, the line indicates the median, and whiskers indicate a 5–95% range. ***p < 0.001.
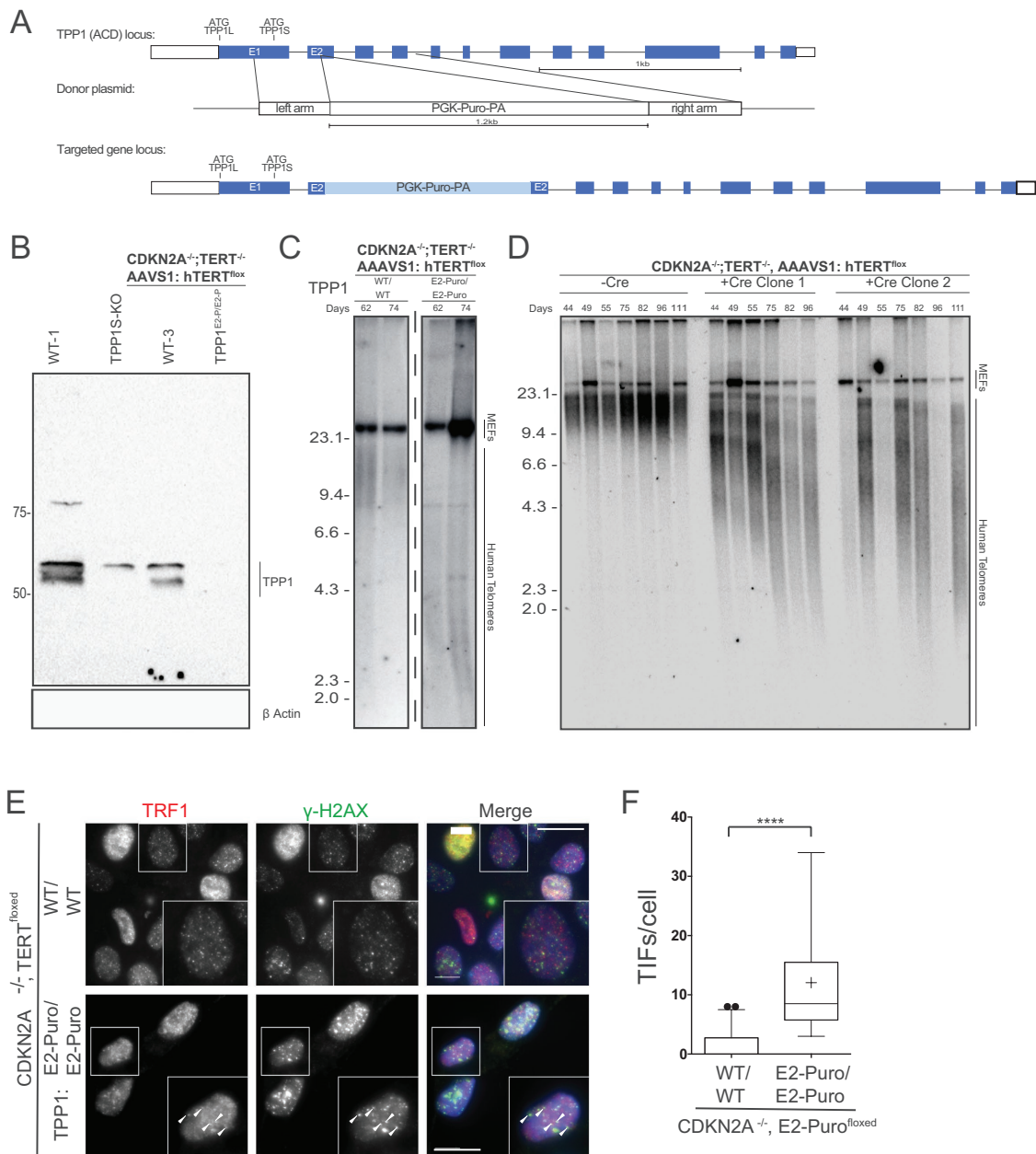
FIGURE 2: Analysis of the complete loss of TPP1 in checkpoint deficient cells. (A) Schematic depicting targeting strategy for knock-in of a puromycin-poly A cassette into exon 2 of TPP1. (B) Western blot analysis of TPP1 gene products in parental cell line and the cell line harboring the exon 2 insertion. WT-1 and TPP1S KO cells used as controls for the gene product. TPP1S KO and control cells were collected 267 following targeting with TPP1S KO cassette. CDKN2A$^{-/-}$ samples were collected 67 d following targeting with TPP1 exon 2 puromycin cassette. Numbers along the side indicate molecular weight in kilodaltons. (C) TRF analysis of TPP1 KO cell line. All samples were run on the same gel; the dashed line indicates a collapsed image. Numbers along the top indicate days following electroporation. Numbers along the side indicate fragment size in kilobases. (D) TRF analysis of parental CDKN2A$^{-/-}$, TERT$^{-/-}$, and AAVS1:TERT^{flox} with and without Cre-mediated loop out of hTERT cassette. Numbers indicate days following transfection with either GFP or Cre mRNA. Numbers along the side indicate fragment size in kilobases. (E) TIF analysis of CDKN2A$^{-/-}$, TERT$^{-/-}$, AAVS1:TERT^{flox} and CDKN2A$^{-/-}$, TERT$^{-/-}$, TPP1$^{E2–Puro/E2–Puro}$, and AAVS1:TERT^{flox} cell lines. Arrows indicate the colocalization of TRF1 and γ-H2Ax foci. Scale bars = 10 μm. Samples were collected 67 d following targeting with TPP1 exon 2 puromycin cassette. (F) Quantification of coincident foci represented in E. Significance was determined by Mann–Whitney test, $n = 44$ CDKN2A$^{-/-}$,TERT^{flox}, TPP1$^{WT/WT}$; $n = 18$ CDKN2A$^{-/-}$,TERT^{flox}, TPP1$^{E2–Puro/E2–Puro}$ cells. Boxes indicate interquartile range, the cross bar indicates median, "+" indicates mean, and whiskers indicate 5–95% range. ****$p < 0.0001$.

Myb domains (TRF1^{ΔAΔM}). In wild-type but not TPP1$^{L104A/L104A}$ cells, overexpression of TRF1^{ΔAΔM} leads to pronounced telomere elongation (Figure 6B and Supplemental Figure S4A).

As TPP1S KO cells showed a severely muted response to telomere lengthening cues, we next investigated to what extent these manipulations could restore telomere protection. Analyzing
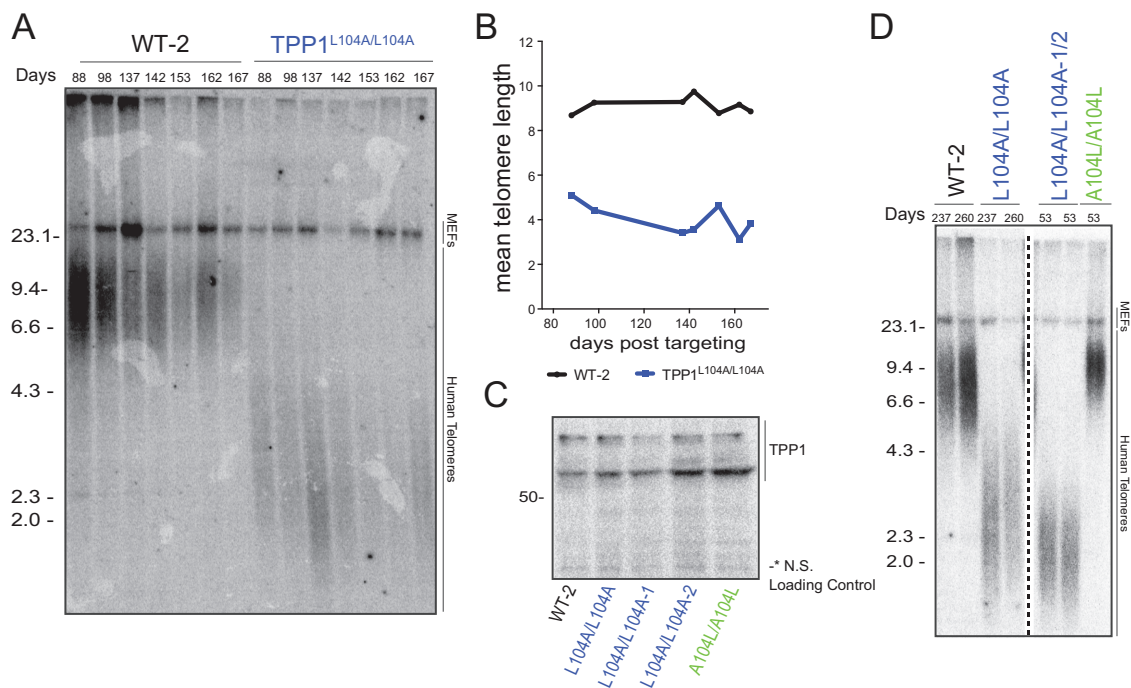
FIGURE 3: Effects of TPP1$^{L104A/L104A}$ mutation on telomere length and end protection. (A) TRF analysis monitoring telomere length changes in wild-type and TPP1$^{L104A/L104A}$ cell lines over time. Numbers along the top indicate days following targeting. Numbers along the side indicate fragment size in kilobases. (B) Quantification of telomere length changes shown in A. (C) Western blot analysis of TPP1 gene products showing endogenous expression of TPP1. *Nonspecific band used as a loading control. Numbers along the side indicate molecular weight in kilodaltons. (D) TRF analysis of telomere length changes following reversion of the TPP1 locus to wild-type, parental mutants, and repaired cell lines. Two unrepaired L104A/L104A clones (indicated by 1/2 in the figure) were isolated following repair targeting and analyzed. Numbers along the top and to the left of the dashed line indicate days following targeting of original L104A mutant. Numbers along the top and to the right of the dashed line indicate days following targeting of the A104L repair. Samples from days 260-left and 53-right were collected on the same day. All samples were run on the same gel; the dashed line indicates a collapsed image. Numbers along the side indicate fragment size in kilobases.

metaphase spreads of TPP1S KO cells revealed a large number of chromosomal and telomere-specific defects in TPP1S KO cells, including telomere signal loss, unbalanced telomere signals, and sister chromatid fusions. In contrast, we did not see a large number of aberrant chromosomes in TPP1$^{L104A/L104A}$ cells. Interestingly, while the expression of either POT1ΔOB or hTERT/hTR in TPP1S KO cells has minimal effect on telomere length, their overexpression is capable of partially suppressing the metaphase phenotypes seen in TPP1S KO cells. (Figure 7, A and B). Telomerase overexpression was more effective at suppressing the chromosome instability than allowing increased telomerase access to telomeres by overexpression of POT1ΔOB. We also examined TIFs in the TPP1S KO cells and found that telomerase expression significantly suppressed the TIF phenotype associated with TPP1S KO cells, while expression of POT1ΔOB was not effective (Figure 7, C and D).

DISCUSSION

### Stem cells express at least two TPP1 isoforms

In our loss of function studies, we have identified specific roles for the different isoforms. hESCs lacking TPP1S are long-term viable, while cells disrupted in all isoforms of TPP1 are not. This argues that hESCs express at least one additional isoform to TPP1S that does not rely on the ATG encoding for M87. These additional TPP1 isoform(s) are sufficient to recruit telomerase and thereby facilitate the immortal phenotype of stem cells but are neither sufficient to maintain telomeres at the stem cell-characteristic telomere length

set point nor to fully ensure telomere protection and genome integrity. It seems worth pointing out the similarity of this phenotype to the adrenocortical dysplasia (acd) mouse. The acd mutant mouse strain has a mutation in intron 3 of TPP1 creating a cryptic splice donor that results in homozygous mice with very low levels of TPP1 expression (approximately 2%) (Else et al., 2007), suggesting that very little TPP1 is required for cellular and organismal viability (Keegan et al., 2005; Hockemeyer et al., 2007). However, KO strategies that fully ablate TPP1 function demonstrate that TPP1 is essential in mice and for the proliferation of mouse keratinocytes, as well as mouse embryonic fibroblasts (Kibe et al., 2010; Tejera et al., 2010).

TPP1S deficiency generally impairs TPP1 functions while the TPP1^{L104A} mutation results in a specific length set point defect

In a second comparison, we contrast the phenotypes of the TPP1S KO to cells with homozygous mutations at amino acid 104 in TPP1. The presence of TIFs and abnormal chromosome ends in TPP1S KO cells revealed that TPP1S is required to properly mediate end protection. This finding is interesting in light of recently published work that indicates that overexpression of TPP1L can suppress TPP1S's telomerase activation function in cancer cell lines, yet does not result in a significant increase in TIFs (Grill et al., 2019). This difference may be the result of impaired DDR in cancer cells when compared with fully intact hESCs with unaltered DDR pathways. TIFs are also
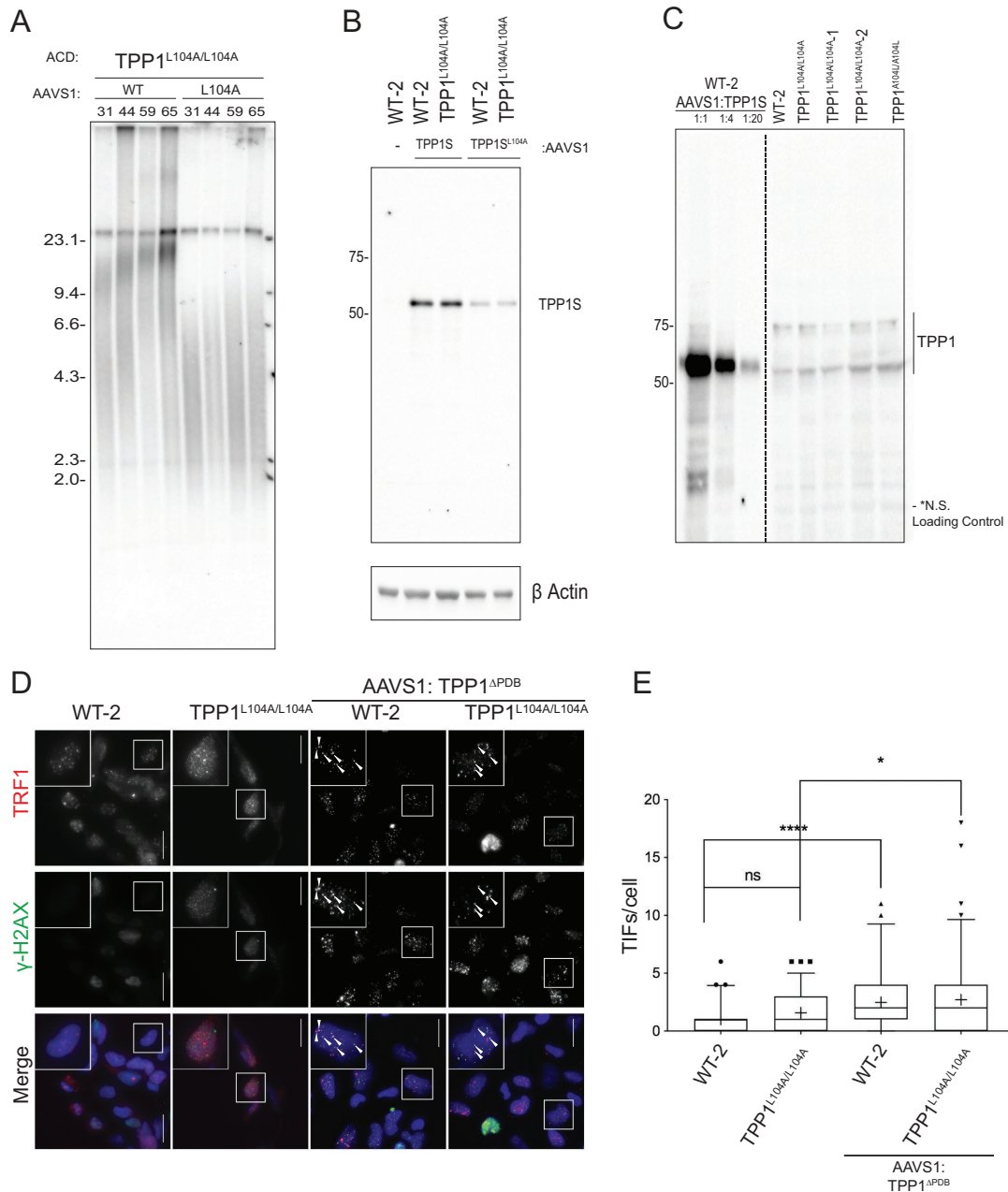
FIGURE 4: Analysis of shelterin overexpression on TPP1$^{L104A/L104A}$. (A) TRF analysis of telomere length following overexpression of TPP1S or TPP1S^{L104A} from the AAVS1 locus. Numbers along the top indicate the days following electroporation of the exogenous TPP1 cassette. Numbers along the side indicate fragment size in kilobases. (B) Western blot analysis of TPP1 overexpression for cell lines in A and Supplemental Figure S3D, lanes 1–13. Samples were collected 32 d postelectroporation of overexpression cassettes. Numbers along the side indicate molecular weight in kilodaltons. (C) Left side, Western blot titration analysis of protein extracts taken from wild-type cells overexpressing TPP1S. Right side, Western blot analysis of wild-type, TPP1^{L104A}, and TPP1^{A104L} repair clones. Samples collected 60 d posttargeting repair of ACD locus. Parental samples were collected on the same day. These data indicated that the overexpression of TPP1S results in an accumulated of more than 20 times greater protein then endogenous TPP1S. The accumulation of TPP1S^{L104A} is an approximately threefold less than that of WT; see B. Thus, there is at least a sixfold increase in protein accumulation following overexpression of TPP1^{L104A} than endogenous TPP1S. Numbers along the side indicate molecular weight in kilodaltons. (D) TIF analysis of wild-type and TPP1$^{L104A/L104A}$ cell lines. TPP1$^{\Delta PDB}$ overexpression cell lines were included as a positive control. Cells were fixed 26 d following targeting the TPP1$^{\Delta PDB}$ expression cassette into the *AAVS1* locus. TPP1$^{\Delta PDB}$ cell lines were generated from parental cell lines that were originally targeted 268 d prior and had stabilized their telomeres. We noticed a reduction in diffuse nucleoplasmic TRF1 staining upon the overexpression of TPP1$^{\Delta PBD}$. This reduction was observed in both wild-type and L104A mutant cell lines. Arrows indicate the colocalization of TRF1 and γ-H2Ax foci. Scale bars = 10 μm. (E) Quantification of coincident foci represented in (D). Significance was determined by Mann–Whitney test, $n = 60$ WT-3, $n = 91$ TPP1$^{L104A/L104A}$, $n = 54$ WT-2; AAVS1: TPP1$^{\Delta PBD}$, and $n = 86$ TPP1$^{L104A/L104A}$; AAVS1: TPP1$^{\Delta PBD}$ cells. Boxes indicate interquartile range, the cross bar indicates median, "+" indicates mean, and whiskers indicate 5–95% range. ****$p < 0.0001$; *$p < 0.05$.
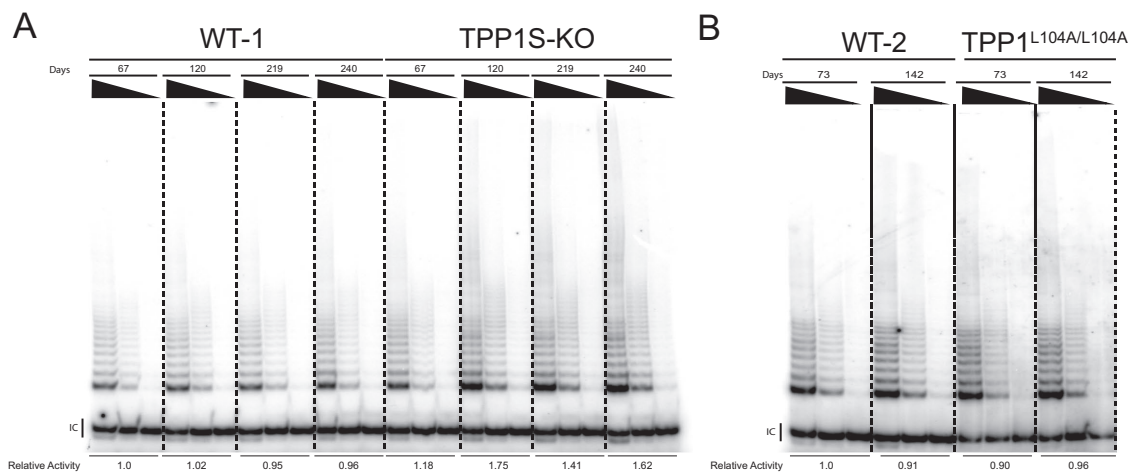
FIGURE 5: Telomerase activity changes in TPP1S KO cells, not TPP1^{L104A} cells. (A) Analysis of telomerase activity by Telomere repeat addition assay (TRAP) in wild-type and TPP1S KO cell lines. Relative activity was determined using ImageJ to calculate total band intensity in the first lane of each time point. Increased activity is evidenced after day 120 in the TPP1S KO cells. Numbers above the radiogram indicate days following targeting M87 generating the TPPS KO. (B) TRAP analysis as in A but of wild type and TPP1$^{L104A/L104A}$. Relative activity was determined as in A. The numbers above the radiogram indicate days following targeting L104A.

absent in hESCs expressing the TPP1^{L104A} mutation, indicating that a TPP1S protein harboring an L104A substitution can properly interact with TIN2 and POT1. These interactions are implied by the fact the TPP1/POT1 heterodimer requires TIN2 for localization to the telomere. Without this localization, telomerase-dependent telomere homeostasis and telomere end protection would be compromised (Ye et al., 2004a; Takai et al., 2011).

During a period of low proliferation and increased cell death in TPP1S KO cells, telomerase activity increases. This increase in activity suggests that cells lacking TPP1S rely on changes in telomerase activity to restore telomere length homeostasis. This delay in up-regulation could be explained by the telomerase's ability to preferentially elongate the shortest telomeres (Greider, 1996; Cristofari and Lingner, 2006; Chiba et al., 2017). This predicts that only after some telomeres become critically short, cells experience a selective pressure to increase telomere maintenance by increasing telomerase activity. In contrast, TPP1$^{L104A/L104A}$ cells can maintain telomeres without a commensurate increase in telomerase activity. The increase of telomerase activity seen in TPP1S KO cells may lead to the saturation of available TPP1. If true, we would predict that TPP1 is limiting in these cells, and the addition of more telomerase or other telomere lengthening cues would have a limited effect on telomere length. This hypothesis was confirmed: in the TPP1S KO cells, we report only a minimal increase in telomere length in response to both of these cues.

In contrast to the TPP1S KO cell results indicative of limiting levels of TPP1, in TPP1$^{L104A/L104A}$ cells, we detected an increase in telomere length following hTERT/hTR or POT1ΔOB overexpression. These data taken together demonstrate that TPP1^{L104A} only shows defects in the establishment of telomere length set point, not other TPP1 roles that are compromised in the TPP1S KO. These results formally establish TPP1 L104 as a dissociation of function mutant.

## What is the defect that causes the altered telomere length set point in L104 cells?

Current studies mostly use overexpression experiments to investigate telomere length control. While this approach allows infer-

ences about how telomeric binding proteins can impact telomere length regulations, the inherent perturbation of the telomere length equilibrium makes it challenging to use these approaches to study how cells establish a telomere length set point and maintain telomeres at homeostasis. To overcome these challenges, we genetically engineered the TPP1^{L104A} mutation at the endogenous locus. This allows us to study the effect of a genetically defined defect in an endogenous shelterin protein in a primary human stem cell line. Our experiments establish that TPP1^{L104A} is competent to protect telomeres, arguing that it properly recruits POT1. The fact that TPP1^{L104A} cells can reestablish telomere length homeostasis, albeit at a shorter set point, demonstrates that the TPP1 can activate telomerase sufficiently to balance out telomere sequence loss. We suggest that the defect in TPP1$^{L104A/L104A}$ is not a defect in telomerase processivity (Nandakumar et al., 2012; Grill et al., 2018). Instead, we suggest that the defect lies in TPP1L104's sensitivity to telomere length feedback information communicated from other shelterin members. Thus, L104A mutation is a separation of function mutant for telomere length set point, independent from its end protection role.

MATERIALS AND METHODS
hESC culture and genome editing

Genome editing experiments were performed in WIBR#3 hESCs (Lengner et al., 2010), National Institutes of Health (NIH) Stem Cell Registry #0079. Cell culture was carried out as previously described (Soldner et al., 2009). For CDKN2A exon2 deletion, the region flanked by accattctgttctctctggc and cgcggaaggtccctcaggtg as sgRNA target sites was removed and genotyped as previously reported (Chiba et al., 2017). For KO and L104A knock-in experiments, cells were coelectroporated with targeting and GFP plasmids, cells were single-cell sorted by florescence-assisted cell sorting, and single cell-derived colonies were isolated, replicate plates were made, and genomic DNA was isolated for confirmation of genotypes. Targeting was confirmed by Sanger sequencing and Southern blot analysis using a probe amplified from genomic DNA using Fw:ggggaaatgatgttggcttagaatcct and Re:caatgaagtccttcgtcttggtca as primers. Southern blot analysis was performed as previously
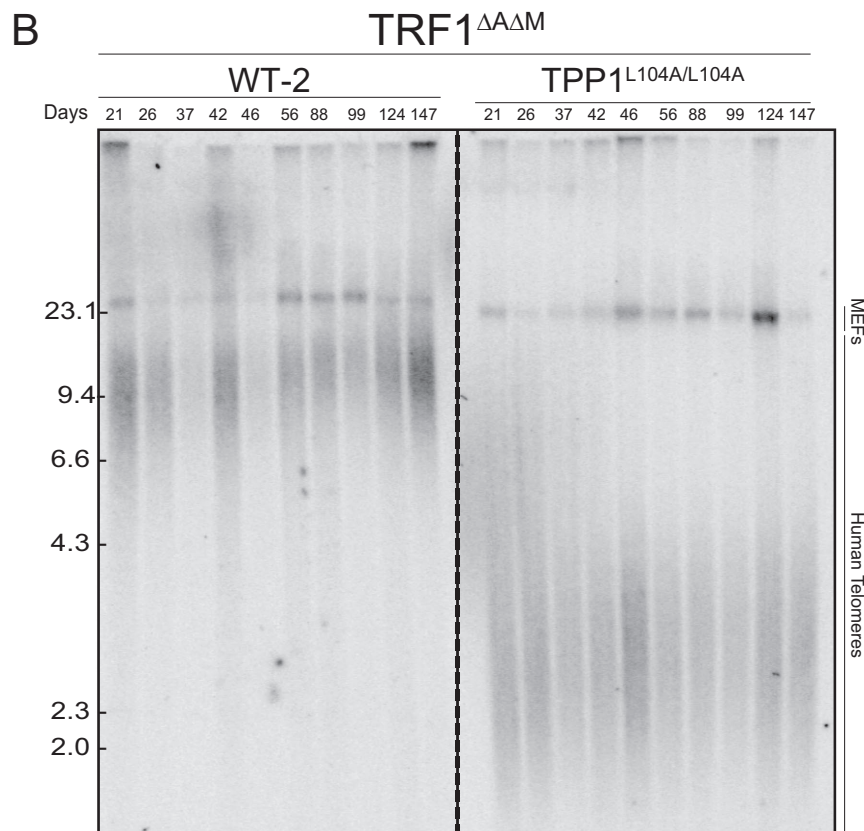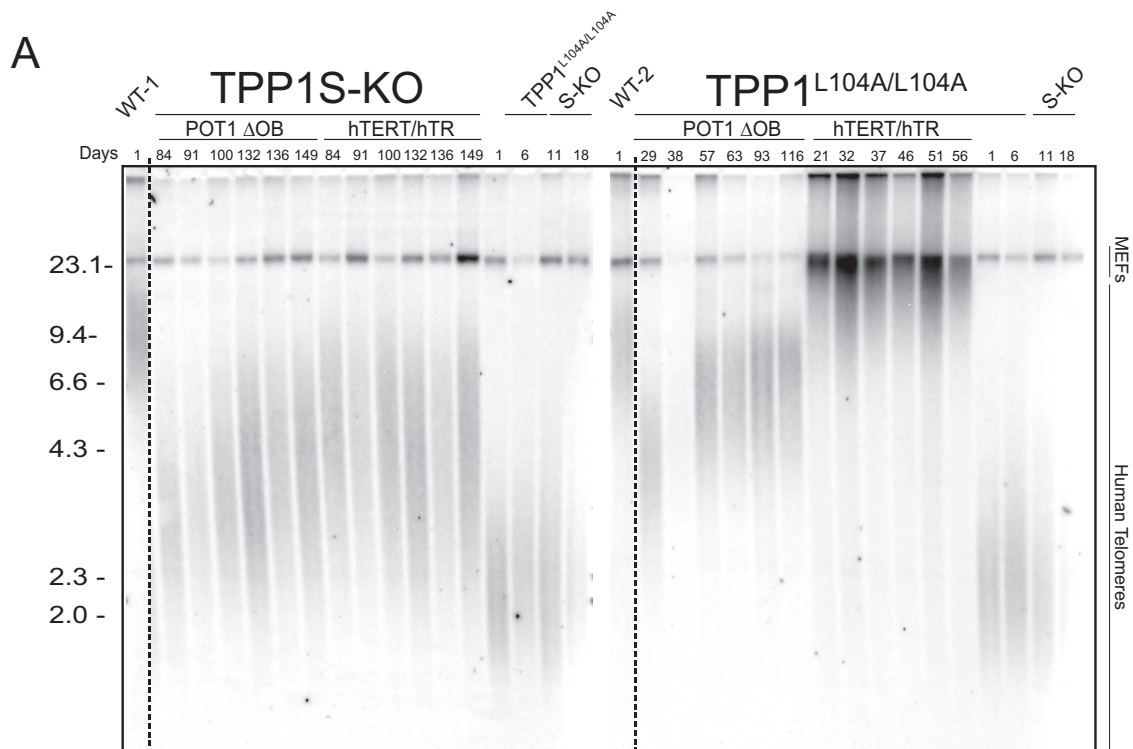
FIGURE 6: Telomere length response of TPP1S KO and TPP1[L104A/L104A] cell lines to lengthening signals. (A) TRF analysis of telomere length changes in wild-type, TPP1S KO, and TPP1[L104A/L104A] cell lines following overexpression of either POT1ΔOB or hTERT/hTR, downstream regulators of telomere length. The TPP1S KO parental cell line, as well as WT-2 control, are synchronized with TPP1S KO overexpression cell lines; day 1 is 164 d postoriginal KO targeting. The TPP1[L104A/L104A] parental cell line as well as the WT-3 control line are synchronized with TPP1[L104A/L104A] overexpression cell
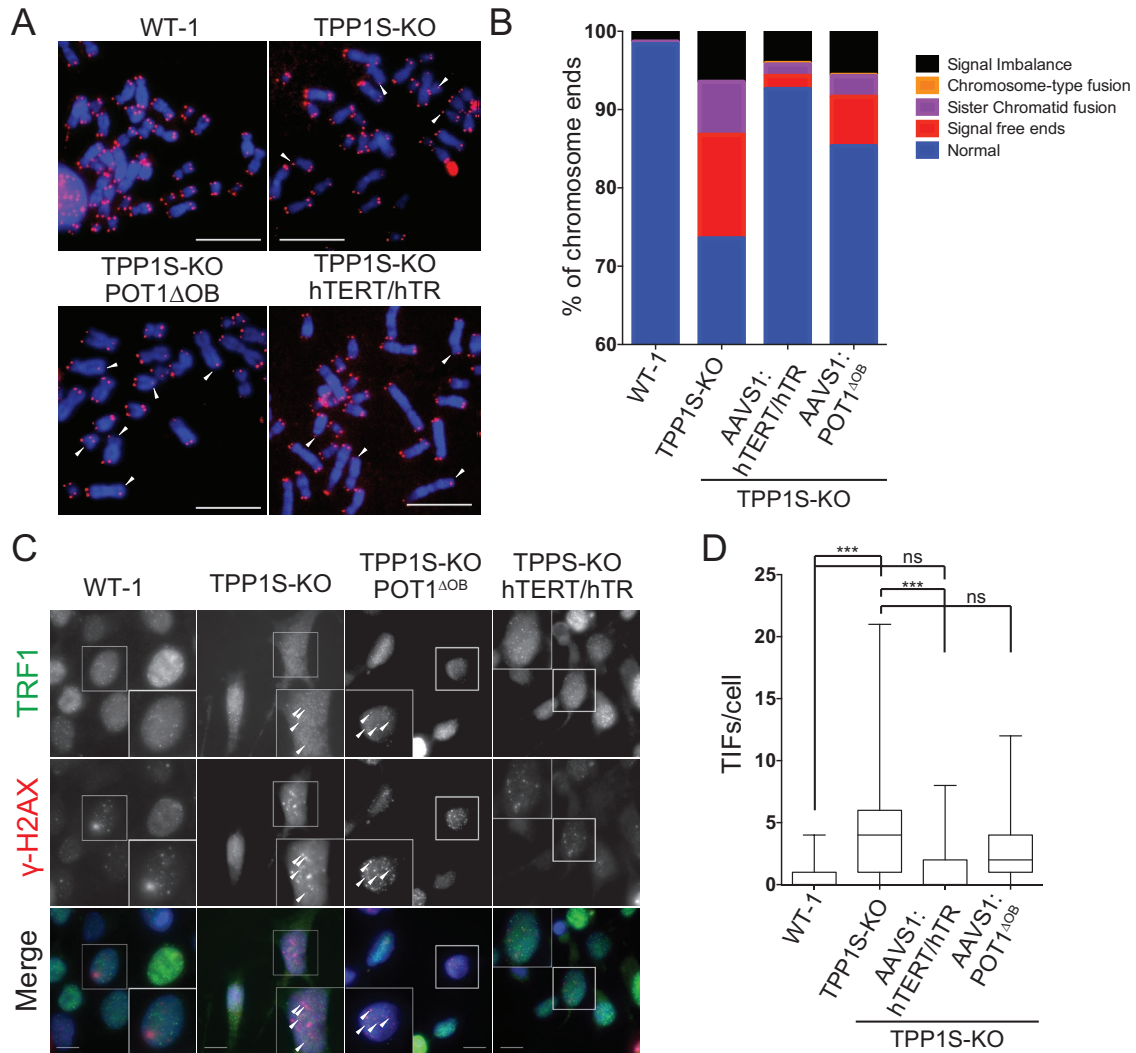
FIGURE 7: Effects of telomerase and POT1ΔOB on telomere end protection in TPP1S KO cells. (A) Metaphase spreads of wild type, TPP1S KO cell line with and without overexpression of either POT1ΔOB or hTERT/hTR. Metaphases were fixed 240 d following targeting for WT-2 and TPP1S KO and day 89 following targeting of the *AAVS1* locus for overexpression cell lines. Metaphases were processed in parallel. Scale bars = 10 μm. (B) Quantification of metaphase spreads represented in A; *n* = 302 WT-1; *n* = 119 TPP1S KO; *n* = 716 TPP1S KO, AAVS1: POT1ΔOB; and *n* = 462 TPP1S KO, AAVS1: hTERT/hTR chromosome ends. Cells were fixed 96 d following targeting of the *AAVS1* locus. (C) TIF analysis of WT-2; TPP1S KO; TPP1S KO, AAVS1:POT1ΔOB; and TPP1S KO, AAVS1:hTERT/hTR cell lines. Arrows indicate the colocalization of TRF1 and γ-H2Ax foci. Scale bars = 10 μm. Samples were collected 105 d after targeting the *AAVS1* locus. (D) Quantification of coincident foci is represented in C. Significance determined by Mann-Whitney test, *n* = 65 WT-1; *n* = 29 TPP1S KO; *n* = 60 TPP1S KO, AAVS1: POT1ΔOB; and *n* = 35 TPP1S KO, AAVS1: hTERT/hTR cells. Boxes indicate interquartile range, cross bar indicates median, "+" indicates mean, and whiskers indicate 5–95% range. ***$p < 0.001$. The data used for columns 1 and 2 are the same as Figure 1I.

described (Hockemeyer *et al.*, 2009, 2011). *AAVS1* targeting was performed as previously described (Sexton *et al.*, 2014). Targeting constructs contained cDNA expressing TPP1S-3xFlag, TPP1ΔPBD-Flag, myc-POT1ΔOB, Flag-hTERT/hTR, Flag-TRF1, or Flag-TRM1ΔAΔM, respectively.

TRAP

PCR-based TRAP was performed as previously described using TS (AATCCGTCGAGCAGAGTT) and ACX (GCGCGGCTTACCCT-TACCCTTACCCTAACC) for amplification of telomeric repeats and TSNT (AATCCGTCGAGCAGAGTTAAAAGGCCGAGAAGCGAT)

lines; day 1 is 136 d postoriginal L104A targeting. All samples were run on two gels; the dashed line indicates a collapsed image. TPP1S KO and TPP1L104A/L104A parental cell lines were added to each gel to allow for a direct comparison of each control. Numbers along the top indicate days following targeting of exogenous cassettes. Numbers along the side indicate fragment size in kilobases. (B) Complementation analysis of TPP1L104A by overexpression of dominant-negative allele of TRF1, TRF1ΔAΔM. Numbers along the top indicate days following targeting of exogenous cassettes. Numbers along the side indicate fragment size in kilobases.

and NT (ATCGCTTCTCGGCCTTTT) as an internal control (Kim et al., 1994).

Cell extracts were generated using Hypotonic Lysis buffer (20 mM HEPES, 2 mM MgCl$_2$, 0.2 mM EGTA, 10% glycerol, 1 mM DTT, 0.1 mM PMSF) supplemented with 0.5% CHAPS. Samples were normalized using the Bradford assay (Bio-Rad). Serial dilutions 200, 40, and 5 ng of whole cell lysate were used to assay telomerase activity. The TRAP products were resolved on 10% polyacrylamide/1× TAE gels. Dried gels were visualized by phosphor imaging.

Immunoblotting

Protein samples were extracted in RIPA buffer, sonicated to liberate chromatin-bound proteins, normalized for protein concentration, and mixed with Laemmli buffer. After heating to 95°C for 5 min, samples were resolved by SDS–PAGE. Proteins were then transferred to nitrocellulose membrane and subsequently incubated with rabbit α-TPP1 (1:1000, A303-069A; Bethyl) and mouse α-Actin (1:20000; Santa Cruz) in 5% nonfat milk (Carnation) in Tris-buffered saline (TBS)-T buffer (150 mM NaCl, 50 mM Tris, pH 7.5, 0.1% Tween 20) overnight at 4°C. The membrane was washed in TBS-T and incubated with goat α–mouse/rabbit HRP (1:5,000; Bio-Rad) in 5% nonfat milk in TBS-T for 1 h at room temperature. After extensive washing with TBS-T, the membrane was visualized using ECL.

Detection of telomere length

Genomic DNA was prepared as described previously (Hockemeyer et al., 2005). Briefly, genomic DNA was digested with MboI, AluI, and RNase A overnight at 37°C. The resulting DNA was normalized, and 2 µg of DNA were run on 0.75% agarose (Seakem ME Agarose, Lonza), dried under vacuum for 2 h at 50°C, and denatured in 0.5 M NaOH, 1.5 M NaCl for 30 min, shaking at 25°C, neutralized with 1 M Tris, pH 6.0, and 2.5 M NaCl shaking at 25°C, 2× for 15 min. Then the gel was prehybridized in Church's buffer (1% bovine serum albumin [BSA], 1 mM EDTA, 0.5 M NaPo$_4$, pH 7.2, 7% SDS) for 1 h at 55°C before adding a ^{32}P-end-labeled (C$_3$TG$_2$)$_3$ telomeric probe. The gel was washed 3 × 30 min in 4× SSC at 50°C and 1 × 30 min in 4× SSC + 0.1% SDS at 25°C before exposing on a phosphor imager screen. Mean telomere length calculations were previously described (Kimura et al., 2010). Specifically, optical density (OD) was determined using ImageJ, and calculations were performed using the formula $\sum((OD_i) * MW_i)/(OD_i)$.

qRT-PCR

RNA was extracted with TRIzol (Lifetech) and treated with DNase I (NEB); 600 ng RNA were converted to cDNA with iScript Reverse Transcriptase (Bio-Rad) using random and poly(A) priming. qRT-PCR was performed with KAPA SYBR fast (KAPA Biosystems) in a 384-well format with a total reaction volume of 10 µl. For measuring the expression levels of GAPDH and OCT4, cDNA was diluted 1:10, and 2 µl were used for qPCR. Relative expression levels were calculated based on Δ/ΔCt and/or ΔCt analysis. qRT-PCR primers used in this study were:

GAPDH fw (CAGTCTTCTGGGTGGCAGTGA), GAPDH rev (CGTGGAAGGACTCATGACCA),

OCT4 fw (CGTTGTGCATAGTCGCTGCT), OCT4 rev (GCTCGAGAAGGATGTGGTCC),

sgRNAs

TPP1S KO: gtgtagccgtggggatggca; TPP1L KO: tgacgaacggcccaaatgcc; TPP1^{L104A}: ctggattcgggagctgattc, TPP1 KO: ccctgatacgtccgacgtcg. The TPP1 KO strategy to disrupt both isoforms has been

independently validated in the HCT116 cancer cell line (Vogan et al., unpublished data).

IF/TIF analysis

For analysis by IF, cells were washed with phosphate-buffered saline (PBS), fixed with 3.7% formaldehyde in PBS, permeabilized, and blocked with PBS + 1 mg/ml BSA, 3% vol/vol horse serum, 0.1% Triton X-100, and 1 mM EDTA. Fixed cells were incubated with antibodies against TRF1 raised in rabbit against amino acid residues 17–41 (856-R1) and γ-H2AX (Millipore) in blocking solution followed by secondary antibodies. The scoring of TIF-positive cells was performed single-blind. Box plots show scoring of 9–11 fields of view and present median, mean, 95% confidence interval, and outliers; p values were determined using Prism 7's Mann–Whitney test. Note the analysis performed in Figures 1I and 4E have been done in parallel.

Metaphase spreads/FISH

Cells were treated with colcemid at 100 µg/ml for 2 h. We collected the cells using trypsin and incubated at 37°C in prewarmed 75 mM KCl. The cells were spun down, and the KCl was removed. Cells were slowly resuspended in a fixative of 3:1 methanol:acetic acid. Cells were stored overnight at 4°C. The next day, cells were spread, dropwise, onto microscope slides and washed twice with 3:1 methanol:acetic acid solution. Slides were then placed onto a 70°C humidified heat block for 1 min.

Telomeres were detected by a previously described protocol (Lansdorp et al., 1996) with a few minor changes. We fixed slides in 4% PFA diluted in PBS, then treated with pepsin (1 mg/ml) prepared in 10 mM glycine, pH 2, and warmed up to 37°C. After one more wash in 4% PFA, slides were washed with PBS, then dehydrated in an ethanol series. Each slide received 70 µl of hybridization mixture and was denatured at 65°C for 5 min and then hybridized overnight with a Cy3 Tel-C PNA probe (PNA Bio) at room temperature in a hybridization chamber. The next day, the slides were washed with 70% formamide, 10 mM Tris-HCl, pH 7.2, 0.1% BSA solution, and then with 0.1 M Tris-HCl, pH 2, 0.15 M NaCl, 0.08% Tween, with DAPI (diluted 1:1000 from 10 mg/ml stock) added to the second wash. Coverslips were mounted with ProLong Gold Antifade Mountant (Thermo Fisher Scientific). All microscopy (IF and metaphase spreads) were imaged on a Nikon Eclipse TE2000-E epifluorescent microscope equipped with an Andor Zyla sCMOS camera.

REFERENCES

Aubert G, Lansdorp PM (2008). Telomeres and aging. Physiol Rev 88, 557–579.

Batista LF, Artandi SE (2013). Understanding telomere diseases through analysis of patient-derived iPS cells. Curr Opin Genet Dev 23, 526–533.

Batista LFZ, Pech MF, Zhong FL, Nguyen HN, Xie KT, Zaug AJ, Crary SM, Choi J, Sebastiano V, Cherry A, et al. (2011). Telomere shortening and loss of self-renewal in dyskeratosis congenita induced pluripotent stem cells. Nature 474, 399–402.

Blair JD, Hockemeyer D, Doudna JA, Bateup HS, Floor SN (2017). Widespread translational remodeling during human neuronal differentiation. Cell Rep 21, 2005–2016.

Bryan TM, Englezou A, Dunham MA, Reddel RR (1998). Telomere length dynamics in telomerase-positive immortal human cell populations. Exp Cell Res 239, 370–378.

Ceccarelli M, Barthel FP, Malta TM, Sabedot TS, Salama SR, Murray BA, Morozova O, Newton Y, Radenbaugh A, Pagnotta SM, et al. (2016). Molecular profiling reveals biologically discrete subsets and pathways of progression in diffuse glioma. Cell 164, 550–563.

Chiba K, Johnson JZ, Vogan JM, Wagner T, Boyle JM, Hockemeyer D (2015). Cancer-associated TERT promoter mutations abrogate telomerase silencing. Elife 4.

Chiba K, Lorbeer FK, Shain AH, McSwiggen DT, Schruf E, Oh A, Ryu J, Darzacq X, Bastian BC, Hockemeyer D (2017). Mutations in the promoter of the telomerase gene TERT contribute to tumorigenesis by a two-step mechanism. Science 357, 1416–1420.

Cristofari G, Lingner J (2006). Telomere length homeostasis requires that telomerase levels are limiting. EMBO J 25, 565–574.

d'Adda di Fagagna F, Reaper PM, Clay-Farrace L, Fiegler H, Carr P, Von Zglinicki T, Saretzki G, Carter NP, Jackson SP (2003). A DNA damage checkpoint response in telomere-initiated senescence. Nature 426, 194–198.

de Lange T (2005). Shelterin: the protein complex that shapes and safeguards human telomeres. Genes Dev 19, 2100–2110.

de Lange T (2010). How shelterin solves the telomere end-protection problem. Cold Spring Harb Symp Quant Biol 75, 167–177.

Else T, Theisen BK, Wu Y, Hutz JE, Keegan CE, Hammer GD, Ferguson DO (2007). Tpp1/Acd maintains genomic stability through a complex role in telomere protection. Chromosome Res 15, 1001–1013.

Floor SN, Doudna JA (2016). Tunable protein synthesis by transcript isoforms in human cells. Elife 5.

Greider CW (1996). Telomere length regulation. Annu Rev Biochem 65, 337–365.

Greider CW, Blackburn EH (1985). Identification of a specific telomere terminal transferase activity in tetrahymena extracts. Cell 43, 405–413.

Greider CW, Blackburn EH (1989). A telomeric sequence in the RNA of Tetrahymena telomerase required for telomere repeat synthesis. Nature 337, 331.

Grill S, Bisht K, Tesmer VM, Shami AN, Hammoud SS, Nandakumar J (2019). Two separation-of-function isoforms of human TPP1 dictate telomerase regulation in somatic and germ cells. Cell Rep 27, 3511–3521.e3517.

Grill S, Tesmer VM, Nandakumar J (2018). The N terminus of the OB domain of telomere protein TPP1 is critical for telomerase action. Cell Rep 22, 1132–1140.

Harley CB, Futcher AB, Greider CW (1990). Telomeres shorten during ageing of human fibroblasts. Nature 345, 458–460.

Hayflick L (1965). The limited in vitro lifetime of human diploid cell strains. Exp Cell Res 37, 614–636.

Hayward NK, Wilmott JS, Waddell N, Johansson PA, Field MA, Nones K, Patch AM, Kakavand H, Alexandrov LB, Burke H, et al. (2017). Whole-genome landscapes of major melanoma subtypes. Nature 545, 175–180.

Hemann MT, Hackett J, Ijpma A, Greider CW (2000). Telomere length, telomere-binding proteins, and DNA damage signaling. Cold Spring Harb Symp Quant Biol 65, 275–279.

Hockemeyer D, Collins K (2015). Control of telomerase action at human telomeres. Nat Struct Mol Biol 22, 848–852.

Hockemeyer D, Palm W, Else T, Daniels JP, Takai KK, Ye JZ, Keegan CE, de Lange T, Hammer GD (2007). Telomere protection by mammalian Pot1 requires interaction with Tpp1. Nat Struct Mol Biol 14, 754–761.

Hockemeyer D, Sfeir AJ, Shay JW, Wright WE, de Lange T (2005). POT1 protects telomeres from a transient DNA damage response and determines how human chromosomes end. EMBO J 24, 2667–2678.

Hockemeyer D, Soldner F, Beard C, Gao Q, Mitalipova M, DeKelver RC, Katibah GE, Amora R, Boydston EA, Zeitler B, et al. (2009). Efficient targeting of expressed and silent genes in human ESCs and iPSCs using zinc-finger nucleases. Nat Biotechnol 27, 851–857.

Hockemeyer D, Wang H, Kiani S, Lai CS, Gao Q, Cassady JP, Cost GJ, Zhang L, Santiago Y, Miller JC, et al. (2011). Genetic engineering of human pluripotent cells using TALE nucleases. Nat Biotechnol 29, 731–734.

Houghtaling BR, Cuttonaro L, Chang W, Smith S (2004). A dynamic molecular link between the telomere length regulator TRF1 and the chromosome end protector Trf2. Curr Biol 14, 1621–1631.

Hug N, Lingner J (2006). Telomere length homeostasis. Chromosoma 115, 413–425.

Jinek M, Chylinski K, Fonfara I, Hauer M, Doudna JA, Charpentier E (2012). A programmable dual-RNA-guided DNA endonuclease in adaptive bacterial immunity. Science 337, 816–821.

Keegan CE, Hutz JE, Else T, Adamska M, Shah SP, Kent AE, Howes JM, Beamer WG, Hammer GD (2005). Urogenital and caudal dysgenesis in adrenocortical dysplasia (acd) mice is caused by a splicing mutation in a novel telomeric regulator. Hum Mol Genet 14, 113–123.

Kibe T, Osawa GA, Keegan CE, de Lange T (2010). Telomere protection by TPP1 is mediated by POT1a and POT1b. Mol Cell Biol 30, 1059–1066.

Kim H, Li F, He Q, Deng T, Xu J, Jin F, Coarfa C, Putluri N, Liu D, Songyang Z (2017). Systematic analysis of human telomeric dysfunction using inducible telosome/shelterin CRISPR/Cas9 knockout cells. Cell Discov 3, 17034.

Kim NW, Piatyszek MA, Prowse KR, Harley CB, West MD, Ho PL, Coviello GM, Wright WE, Weinrich SL, Shay JW (1994). Specific association of human telomerase activity with immortal cells and cancer. Science 266, 2011–2015.

Kimura M, Stone RC, Hunt SC, Skurnick J, Lu X, Cao X, Harley CB, Aviv A (2010). Measurement of telomere length by the Southern blot analysis of terminal restriction fragment lengths. Nat Protoc 5, 1596–1607.

Lansdorp PM, Verwoerd NP, van de Rijke FM, Dragowska V, Little MT, Dirks RW, Raap AK, Tanke HJ (1996). Heterogeneity in telomere length of human chromosomes. Hum Mol Genet 5, 685–691.

Lengner CJ, Gimelbrant AA, Erwin JA, Cheng AW, Guenther MG, Welstead GG, Alagappan R, Frampton GM, Xu P, Muffat J, et al. (2010). Derivation of pre-X inactivation human embryonic stem cells under physiological oxygen concentrations. Cell 141, 872–883.

Liu D, Safari A, O'Connor MS, Chan DW, Laegeler A, Qin J, Songyang Z (2004). PTOP interacts with POT1 and regulates its localization to telomeres. Nat Cell Biol 6, 673–680.

Loayza D, de Lange T (2003). POT1 as a terminal transducer of TRF1 telomere length control. Nature 423, 1013–1018.

Marion RM, Strati K, Li H, Tejera A, Schoeftner S, Ortega S, Serrano M, Blasco MA (2009). Telomeres acquire embryonic stem cell characteristics in induced pluripotent stem cells. Cell Stem Cell 4, 141–154.

Nandakumar J, Bell CF, Weidenfeld I, Zaug AJ, Leinwand LA, Cech TR (2012). The TEL patch of telomere protein TPP1 mediates telomerase recruitment and processivity. Nature 492, 285–289.

Rivera T, Haggblom C, Cosconati S, Karlseder J (2016). A balance between elongation and trimming regulates telomere stability in stem cells. Nat Struct Mol Biol 24, 30–39.

Schmidt JC, Dalby AB, Cech TR (2014). Identification of human TERT elements necessary for telomerase recruitment to telomeres. Elife 3.

Schmutz I, de Lange T (2016). Shelterin. Curr Biol 26, R397–R399.

Sexton AN, Regalado SG, Lai CS, Cost GJ, O'Neil CM, Urnov FD, Gregory PD, Jaenisch R, Collins K, Hockemeyer D (2014). Genetic and molecular identification of three human TPP1 functions in telomerase action: recruitment, activation, and homeostasis set point regulation. Genes Dev 28, 1885–1899.

Shay JW (2016). Role of telomeres and telomerase in aging and cancer. Cancer Discov 6, 584–593.

Smogorzewska A, van Steensel B, Bianchi A, Oelmann S, Schaefer MR, Schnapp G, de Lange T (2000). Control of human telomere length by TRF1 and TRF2. Mol Cell Biol 20, 1659–1668.

Soldner F, Hockemeyer D, Beard C, Gao Q, Bell GW, Cook EG, Hargus G, Blak A, Cooper O, Mitalipova M, et al. (2009). Parkinson's disease patient-derived induced pluripotent stem cells free of viral reprogramming factors. Cell 136, 964–977.

Takahashi K, Tanabe K, Ohnuki M, Narita M, Ichisaka T, Tomoda K, Yamanaka S (2007). Induction of pluripotent stem cells from adult human fibroblasts by defined factors. Cell 131, 861–872.

Takai KK, Kibe T, Donigian JR, Frescas D, de Lange T (2011). Telomere protection by TPP1/POT1 requires tethering to TIN2. Mol Cell 44, 647–659.

Teixeira MT, Arneric M, Sperisen P, Lingner J (2004). Telomere length homeostasis is achieved via a switch between telomerase- extendible and -nonextendible states. Cell 117, 323–335.

Tejera AM, Stagno d'Alcontres M, Thanasoula M, Marion RM, Martinez P, Liao C, Flores JM, Tarsounas M, Blasco MA (2010). TPP1 is required for TERT recruitment, telomere elongation during nuclear reprogramming, and normal skin development in mice. Dev Cell 18, 775–789.

Thomson JA, Itskovitz-Eldor J, Shapiro SS, Waknitz MA, Swiergiel JJ, Marshall VS, Jones JM (1998). Embryonic stem cell lines derived from human blastocysts. Science 282, 1145–1147.

van Steensel B, de Lange T (1997). Control of telomere length by the human telomeric protein TRF1. Nature 385, 740–743.

Wang F, Podell ER, Zaug AJ, Yang Y, Baciu P, Cech TR, Lei M (2007). The POT1–TPP1 telomere complex is a telomerase processivity factor. Nature 445, 506–510.

Xin H, Liu D, Wan M, Safari A, Kim H, Sun W, O'Connor MS, Songyang Z (2007). TPP1 is a homologue of ciliate TEBP-β and interacts with POT1 to recruit telomerase. Nature 445, 559.

Ye JZ-S, Hockemeyer D, Krutchinsky AN, Loayza D, Hooper SM, Chait BT, de Lange T (2004a). POT1-interacting protein PIP1: a telomere length regulator that recruits POT1 to the TIN2/TRF1 complex. Genes Dev 18, 1649–1654.

Ye JZS, Hockemeyer D, Krutchinsky AN, Loayza D, Hooper SM, Chait BT, de Lange T (2004b). POT1-interacting protein PIP1: a telomere length regulator that recruits POT1 to the TIN2/TRF1 complex. Genes Dev 18, 1649–1654.

Zhong FL, Batista LFZ, Freund A, Pech MF, Venteicher AS, Artandi SE (2012). TPP1 OB-fold domain controls telomere maintenance by recruiting telomerase to chromosome ends. Cell 150, 481–494.